Inorg. Chem. **2006**, *45*, 108–118

Analysis of Weak Interactions in the Crystal Packing of Inorganic Metalorganic Hybrids Based on Keggin Polyoxometalates and Dinuclear Copper(II)–Acetate Complexes

Santiago Reinoso, Pablo Vitoria, Leire San Felices, Luis Lezama,* and Juan M. Gutiérrez-Zorrilla*

Departamento de Química Inorgánica, Facultad de Ciencia y Tecnología, Universidad del País Vasco, P.O. Box 644, E-48080 Bilbao, Spain

Received August 3, 2005

Reaction of in situ generated copper-monosubstituted Keggin polyoxometalate (POM) and copper–phenanthroline complexes in potassium or sodium acetate buffers led to the formation of the potassium salt of $[\{SiW_{11}O_{39}Cu(H_2O)\}\{Cu_2(phen)_2(H_2O)(ac)_2\}]^{4-}$ (**1**) and $[\{Si_2W_{22}Cu_2O_{78}(H_2O)\}\{Cu_2(phen)_2(H_2O)(ac)_2\}_2]^{8-}$ (**2**, where phen = phenanthroline and ac = acetate) hybrid polyanions, respectively. Both compounds are the first discrete mono- and bimolecular transition-metal-substituted Keggin POMs that support a binuclear copper–acetate complex. Despite the different nature of the POMs, the crystal packing of the two compounds is closely related, being formed of hybrid parallel layers that give rise to an alternate sequence of inorganic and metalorganic regions. This packing type seems to be determined by the extensive network of weak intermolecular interactions established by the dicopper complexes, as a Hirshfeld surface analysis shows. Electron paramagnetic resonance studies indicate that both the supported $[Cu_2(ac)_2(phen)_2(H_2O)]^{2+}$ complexes and the copper(II)-monosubstituted POMs are magnetically isolated.

Introduction

The contemporary interest in the chemistry of polyoxometalates[1] (POMs) not only stems from their applications in fields such as medicine,[2] material science,[3] and catalysis[4] but also stems from their intriguing variety of architectures and topologies. The incorporation of metalorganic moieties into inorganic oxide clusters provides a powerful method for structural modification and synthesis of novel metalorganic−inorganic hybrid materials that combine the features of both substructures. Several research groups are involved in the preparation of organic−inorganic hybrids based on POMs.[5]

It has long been recognized that the ability to functionalize POM anions would extend their versatility and lead to new

* To whom correspondence should be addressed. E-mail: juanma.zorrilla@ehu.es (J.M.G.-Z.), luis.lezama@ehu.es (L.L.).

(1) (a) Hill, C. L., Ed. *Chem. Rev.* **1998**, *98*, 1 (special thematic issue). (b) Pope, M. T., Müller, A., Eds. *Polyoxometalate Chemistry: From Topology via self-Assembly to Applications*; Kluwer: Dordrecht, Germany, 2001. (c) Pope, M. T., Yamase, T., Eds. *Polyoxometalate Chemistry for Nanocomposite Design*; Kluwer: Dordrecht, Germany, 2002. (d) Borrás-Almenar, J. J., Coronado, E., Müller, A., Pope M. T., Eds. *Polyoxometalate Molecular Science*; Kluwer: Dordrecht, Germany, 2003.

(2) (a) Michelon, M.; Hervé, M.; Hervé, G. *Biochim. Biophys. Acta* **1987**, *916*, 402. (b) Chottard, G.; Hill, C. L.; Weeks, M. S.; Schinazi, R. F. *J. Med. Chem.* **1990**, *33*, 2767. (c) Inouye, Y.; Tale, Y.; Tokutake, Y.; Yoshida, T.; Yamamoto, A.; Yamase, T.; Nakamura, S. *Chem. Pharm. Bull.* **1990**, *38*, 285. (d) Barnard, D. L.; Hill, C. L.; Gage, T.; Matheson, J. E.; Huffman, J. H.; Sidwell, R.; Otto, M. I.; Schinazi, R. F. *Antiviral Res.* **1997**, *34*, 27. (e) Fukuda, N.; Yamase, T.; Tajima, Y. *Biol. Pharm. Bull.* **1999**, *22*, 463. (f) Rhule, J. T.; Hill, C. L.; Zheng, Z.; Schinazi, R. F. *Top. Biol. Inorg. Chem.* **1999**, *2*, 117. (g) Wang, X.; Liu, J.; Li, J.; Yang, Y.; Liu, J.; Li, B.; Pope, M. T. *J. Inorg. Biochem.* **2003**, *94*, 279. (h) Wang, X.; Liu, J.; Pope, M. T. *Dalton Trans.* **2003**, 957.

(3) (a) Gómez-García, C. J.; Coronado, E.; Ouahab, L. *Angew. Chem., Int. Ed. Engl.* **1992**, *31*, 240. (b) Coronado, E.; Gómez-García, C. J. *Comments Inorg. Chem.* **1995**, *17*, 255. (c) Clemente-Juan, J. M.; Coronado, E. *Coord. Chem. Rev.* **1999**, *193*−*195*, 361. (d) Mialane, P.; Dolbecq, A.; Marrot, J.; Rivière, E.; Sécheresse, F. *Angew. Chem., Int. Ed.* **2004**, *43*, 2274. (e) Forment-Aliaga, A.; Coronado, E.; Feliz, M.; Gaita-Ariño, A.; Llusar, R.; Romero, F. M. *Inorg. Chem.* **2004**, *43*, 8019. (f) Casañ-Pastor, N.; Gómez-Romero P. *Front. Biosci.* **2004**, *9*, 1759. (g) Mialane, P.; Dolbecq, A.; Marrot, J.; Rivière, E.; Sécheresse, F. *Chem.*−*Eur. J.* **2005**, *11*, 1771.

(4) (a) Okuhara, T.; Mizuno, N.; Misono, M. *Adv. Catal.* **1996**, *41*, 113. (b) Neumann, R. *Prog. Inorg. Chem.* **1998**, *47*, 317. (c) Kuznetsova, L. I.; Maksimov, G. M.; Likholobov, V. A. *Kinet. Catal.* **1999**, *40*, 622. (d) Misono, M. *Chem. Commun.* **2001**, 1141. (e) Khenkin, A. M.; Weiner, L.; Wang, Y.; Neumann, R. *J. Am. Chem. Soc.* **2001**, *123*, 8531. (f) Kozhevnikov, I. V. *Catalysis by Polyoxometalates*; Catalysts for Fine Chemicals; Wiley: Chichester, U.K., 2002; Vol. 2. **(g)** Kiricsi, I., Ed. *Appl. Catal., A* **2003**, *256*, 1 (special issue). (h) Hill, C. L. *Angew. Chem., Int. Ed.* **2004**, *43*, 402. (i) Liu, H.; Iglesia, E. *J. Catal.* **2004**, *223*, 161. (j) Stahl, S. S. *Angew. Chem., Int. Ed.* **2004**, *43*, 3400. (k) Won, B. K.; Voitl, T.; Rodríguez-Rivera, G. J.; Dumesic, J. A. *Science* **2004**, *305*, 1280.

10.1021/ic051322c CCC: $33.50
Published on Web 11/11/2005

and more selective applications. Thus, the possibility of combining metalorganic complexes and POMs gives up a hybrid compound with two functional centers, which was used as an effective hydrogenation catalyst.[6] The chemistry of POM-based hybrids has been significantly enriched by the inclusion of transition-metal (TM) coordination complexes in the hybrid system, either to provide charge compensation or to be a part of the inorganic POM framework itself.[7]

Currently, we are exploring the applicability of TM-monosubstituted Keggin POMs and TM−carboxylate cationic complexes for the synthesis of new magnetically attractive hybrid compounds by self-assembly processes of the inorganic and metalorganic building blocks generated in situ[8] as an alternative to the hydrothermal techniques that are generally employed. Furthermore, we are interested in the analysis of the weak interactions and their influence on packing modes.

A recently developed method by Spackman et al.[9] for the study of intermolecular interactions is the use of graphical plots of the Hirshfeld surfaces mapped with various properties. These surfaces encode information about all intermolecular interactions simultaneously, and they provide a powerful tool for elucidating and comparing intermolecular interactions as well as for spotting common features and trends in specific classes of compounds. The Hirshfeld surface is a means of partitioning space in a crystal into regions where the contribution from the electron distribution of a sum of spherical atoms for the molecule (the promolecule) exceeds the contribution from the corresponding sum over the rest of the crystal. Surface characteristics reflect the interplay between different atomic sizes and intermolecular contact distances and, hence, intermolecular interactions, in a very subtle way.

Various properties can be encoded on the surfaces. The simplest and most immediately useful property to map is the distance from the surface to the nearest nucleus external to the surface (d_e), which provides an immediate picture of the nature of intermolecular contacts in the crystal. Two other properties which can give chemical insight are the *curvedness* (*C*) and the *shape index* (*S*), both related to the surface curvature and, thus, to its shape. Areas on the Hirshfeld surface with high curvedness tend to divide the surface into contact patches with each neighboring molecule so that the curvedness of the Hirshfeld surface could be used to define a coordination number in the crystal. The shape index is a qualitative measure of shape and can be sensitive to very subtle changes in surface shape, particularly in regions where the curvedness is very low. One important attribute of the shape index is that two shapes, where the shape index differs only by a sign, represent complementary "stamp" and "mold" pairs. This means that maps of the shape index on the Hirshfeld surface can be used to identify complementary hollows and bumps.

Here we report the synthesis, magnetic properties, and the structural study using Hirshfeld surfaces of the following hybrid compounds: $K_4[\{SiW_{11}O_{39}Cu(H_2O)\}\{Cu_2(ac)_2(phen)_2(H_2O)\}]\cdot 14H_2O$ (**1**) and $K_8[\{Si_2W_{22}Cu_2O_{78}(H_2O)\}\{Cu_2(ac)_2(phen)_2(H_2O)\}_2]\cdot\sim 40H_2O$ (**2**, where phen = phenanthroline and ac = acetate), which represent a nice example of how weak interactions affecting the dicopper complexes, either among themselves or with the inorganic component, determine the crystal packing, regardless of the exact nature of the inorganic POM.

Experimental Section

Materials and Methods. All reagents were used as purchased without further purification. The $K_8[\alpha\text{-}SiW_{11}O_{39}]$ precursor was synthesized as described in the literature.[10] Infrared spectra for solid samples were obtained as KBr pellets on a Mattson 1000 Fourier transform infrared spectrometer. The magnetic susceptibility was measured on a Quantum Design MPMS-7 SQUID magnetometer (T range = 5−300 K, applied field = 0.1 T, diamagnetic corrections estimated from Pascal's constants). Electron paramagnetic resonance (EPR) powder spectra were recorded on a Bruker ESP300 spectrometer (X and Q bands) equipped with Oxford low-temperature devices (magnetic field calibration, NMR probe; determination of the frequency inside the cavity, Hewlett-Packard 5352B microwave frequency counter; maintenance of the crystal structures in the powder samples was confirmed by powder X-ray diffraction; computer simulation, WINEPR-Simfonia, version 1.5, Bruker Analytische Messtechnik GmbH). C, H, and N were determined by organic microanalysis on an LECO CHNS-932 analyzer. Cu and K were determined on a Perkin-Elmer 4110ZL atomic absorption spectrometer.

Synthesis of $K_4[\{SiW_{11}O_{39}Cu(H_2O)\}\{Cu_2(ac)_2(phen)_2(H_2O)\}]\cdot 14H_2O$ (1). To an aqueous solution of $CuCl_2\cdot H_2O$ (34 mg, 0.2 mmol) was added 40 mL of an acetic acid/potassium acetate buffered solution of $K_8[SiW_{11}O_{39}]\cdot 13H_2O$ (644 mg, 0.2 mmol). The resulting cloudy solution was heated and stirred for 30 min. A water/methanol solution of $CuCl_2\cdot H_2O$ (68 mg, 0.4 mmol) and 1,10-phenanthroline (79 mg, 0.4 mmol) was then added dropwise, and a pale blue precipitate appeared. The resulting suspension was stirred overnight, and then the precipitate was removed by filtration. Prismatic blue single crystals were obtained from the mother liquor by slow evaporation. Yield: 300 mg (40% based on W). IR (KBr pellets, cm^{-1}, acetate): 1518 (m), 1427 (s); 1338 (w). IR (KBr pellets, cm^{-1}, POM): 1005 (m), 947 (s), 899 (vs), 793 (vs), 741 (s), 687 (s), 538 (m). Elem anal. Calcd for $C_{28}H_{26}Cu_3K_4N_4O_{45}SiW_{11}\cdot 14H_2O$: C, 8.88; H, 1.44; N, 1.48; Cu, 4.76; K, 3.99. Found: C, 9.04; H, 1.38; N, 1.44; Cu, 5.03; K, 4.13.

(5) (a) Burkholder, E.; Zubieta, J. *Inorg. Chim. Acta* **2004**, *357*, 301. (b) Bareyt, S.; Piligkos, S.; Hasenknopf, B.; Gouzerh, P.; Lacôte, E.; Thorimbert, S.; Malacria, M. *Angew. Chem., Int. Ed.* **2003**, *42*, 3404. (c) Sazani, G.; Pope, M. T. *Dalton Trans.* **2004**, 1989.

(6) Bar-Nahum, I.; Neumann, R. *Chem. Commun.* **2003**, 2690.

(7) (a) Lin, B.-Z.; Chen, Y.-M.; Liu, P.-D. *Dalton Trans.* **2003**, 2474. (b) Duan, L. M.; Pan, C. L.; Xu, J. Q.; Cui, X. B.; Xie, F. T.; Wang, T. G. *Eur. J. Inorg. Chem.* **2003**, 2578. (c) Yuan, M.; Li, Y. G.; Wang, E. B.; Tian, C. G.; Wang, L.; Hu, C. W.; Hu, N. H.; Jia, H. Q. *Inorg. Chem.* **2003**, *42*, 3670. (d) Liu, C. M.; Luo, J. L.; Zhang, D. Q.; Wang, N. L.; Chen, Z. J.; Zhu, D. B. *Eur. J. Inorg. Chem.* **2004**, 4774. (e) Li, F. Y.; Xu, L.; Wei, Y. G.; Wang, E. B. *Inorg. Chem. Commun.* **2005**, *8*, 263. (f) Liu, C. M.; Zhang, D. Q.; Xu, C. Y.; Zhu, D. B. *Solid State Sci.* **2004**, *6*, 689. (g) Liu, C. M.; Zhang, D. Q.; Xiong, M.; Zhu, D. B. *Chem. Commun.* **2002**, 1416.

(8) (a) San Felices, L.; Vitoria, P.; Gutiérrez-Zorrilla, J. M.; Reinoso, S.; Etxebarria, J.; Lezama, L. *Chem.—Eur. J.* **2004**, *10*, 5138. (b) Reinoso, S.; Vitoria, P.; San Felices, L.; Lezama, L.; Gutiérrez-Zorrilla, J. M. *Chem.—Eur. J.* **2005**, *11*, 1538.

(9) (a) Spackman, M. A.; Byrom, P. G. *Chem. Phys. Lett.* **1997**, 267, 215. (b) McKinnon, J. J.; Spackman, M. A.; Mitchell, A. S. *Acta Crystallogr., Sect. B* **2004**, *60*, 627.

(10) Tézé, A.; Hervé, G. *J. Inorg. Nucl. Chem.* **1977**, *39*, 999.

Scheme 1

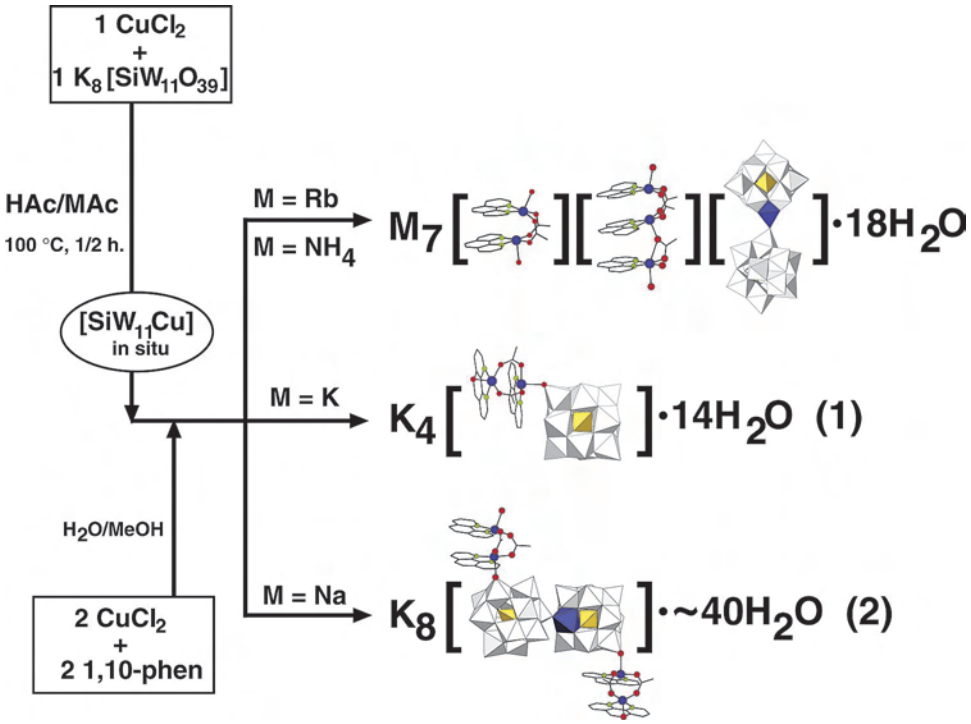

Synthesis of $K_8[\{Si_2W_{22}Cu_2O_{78}(H_2O)\}\{Cu_2(ac)_2(phen)_2(H_2O)\}_2]\cdot\sim 40H_2O$ (2). This compound was prepared by the same method as for **1** but using an acetic acid/sodium acetate buffer solution for the preparation of the POM precursor solution. Yield: 330 mg (45% based on W). IR (KBr pellets, cm^{-1}, acetate): 1520 (m), 1429 (w); 1340 (w). IR (KBr pellets, cm^{-1}, POM): 1007 (m), 949 (s), 901 (vs), 796 (vs), 741 (s), 688 (s), 540 (m). Elem anal. Calcd for $C_{56}H_{50}Cu_6K_8N_8O_{89}Si_2W_{22}\cdot 40H_2O$: C, 8.65; H, 1.69; N, 1.44; Cu, 4.90; K, 4.02. Found: C, 8.40; H, 1.75; N, 1.37; Cu, 4.87; K, 3.95.

X-ray Data Collection and Structure Determination. Data for the single-crystal X-ray studies of **1** and **2** were collected at room temperature on an Xcalibur single-crystal diffractometer (Mo Kα radiation, $\lambda = 0.710\ 73$ Å) fitted with a Sapphire charge-coupled device detector. A total of 1532 (1148) frames of data were collected with an exposure time of 16 s (12 s) per frame, using the ω-scan technique with a frame width of $\Delta\omega = 0.30°$ (0.40°), for compound **1** (**2**). Data frames were processed using the CrysAlis software package.[11] The structures were solved using Patterson methods[12] and refined by full-matrix least-squares analysis with the SHELXL-97 program.[13] All H atoms were included in calculated positions and refined as riding atoms using the default SHELXL parameters. For compound **1**, thermal vibrations were treated anisotropically for W and Cu atoms only. For compound **2**, after locating and refining the hybrid POM, the difference Fourier map showed many peaks of very low electronic density, suggesting an extensive disorder of the water solvent molecules and potassium cations. Thus, the solvent molecules and the countercations that reside in those regions of diffuse electron density were treated by the Platon/Squeeze procedure,[14] which suggested a unit cell accessible volume of about 36%, which could accommodate the 8 expected potassium cations and about 40 water molecules per formula unit. Thermal vibrations were treated anisotropically for W, Cu, Si, and POM O atoms. All calculations were performed using the WinGX crystallographic software package.[15] The final geometrical calculations and the graphical manipulations were carried out with the PLATON program.[16]

Hirshfeld surface plots were obtained using the program Crystal Explorer.[17]

Results and Discussion

Synthesis. The final product of the reaction between copper-monosubstituted Keggin POM and copper−phenanthroline complexes in acetic acid/alkaline acetate buffer solutions is strongly dependent on the alkaline cation. Thus, four different hybrid compounds based on $[SiW_{11}O_{39}Cu(H_2O)]^{6-}$ anions and $[\{Cu(phen)(H_2O)\}_2(ac)_2]^{2+}$ dimers are obtained if the reaction is carried out under the same open air conditions but varying the alkaline cation from sodium to rubidium. When Rb^+ or NH_4^+ acetate buffers are used, the dicopper complex remains as a countercation to give ionic compounds of the formula $A_7[Cu_2(ac)_2(phen)_2(H_2O)_2][Cu_3(ac)_3(phen)_3(H_2O)_3][Si_2W_{22}Cu_2O_{78}(H_2O)]\cdot\sim 18H_2O$ ($A = NH_4^+$, Rb^+).[8b] On the other hand, in the research described in this article, using K^+ or Na^+ acetate media, the dimers get anchored to the Keggin subunits to give the discrete hybrid polyanions contained in compounds **1** and **2**, respectively (Scheme 1). This fact indicates that the cationic dimer $[\{Cu(phen)(H_2O)\}_2(ac)_2]^{2+}$ shows a low tendency to coordinate

(11) *CrysAlis CCD and RED*, Version 1.70; Oxford Diffraction, Ltd.: Oxford, U.K., 2003.
(12) Altomare, A.; Burla, M. C.; Camalli, M.; Cascarano, G. L.; Giacovazzo, C.; Guagliardi, A.; Moliterni, A. G. G.; Polidori, G.; Spagna, R. *J. Appl. Crystallogr.* **1999**, *32*, 115.
(13) Sheldrick, G. M. *SHELXL97*; University of Göttingen: Göttingen, Germany, 1999.
(14) Spek, A. L. *J. Appl. Crystallogr.* **2003**, *36*, 7.
(15) Farrugia, L. J. *J. Appl. Crystallogr.* **1999**, *32*, 837.
(16) Spek, A. L. *PLATON*; Utrecht University: Utrecht, The Netherlands, 2001.
(17) Grimwood, D.; Wolff, S. K.; McKinnon, J.; Spackman, M.; Jayatilaka, D. *Crystal Explorer*, Version 1.0.3; University of Western Australia: Crawley, Australia, 2004.

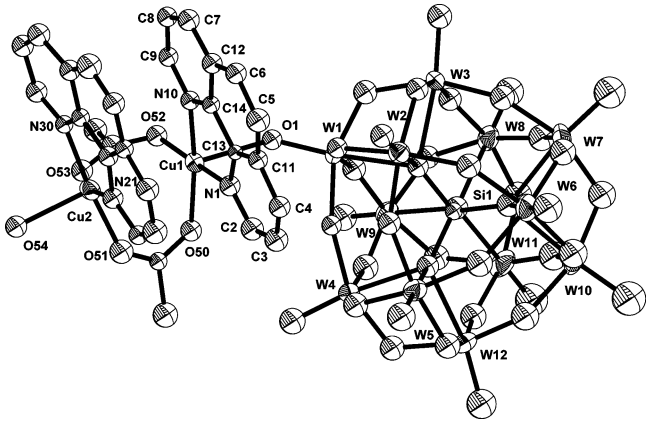

Figure 1. ORTEP view of metalorganic−POM hybrid of compound **1** with atom labeling.

Table 1. X-ray Crystallographic Data for Compounds **1** and **2**

	1	**2**
empirical formula	$C_{28}H_{54}Cu_3K_4N_4O_{59}SiW_{11}$	$C_{56}H_{130}Cu_6K_8N_8O_{129}Si_2W_{22}$
fw	3788.2	7774.6
space group	$P2_1/c$	$C2/c$
a, Å	22.128(2)	47.000(2)
b, Å	12.524(2)	12.7895(8)
c, Å	26.660(2)	26.3943(9)
β, deg	91.617(7)	90.270(3)
V, Å^3	7385(2)	15 865(1)
Z	4	4
T, K	293(1)	293(1)
D_{calc}, g·cm^{-3}	3.407(1)	3.255(1)
μ, mm^{-1}	18.250	17.001
θ limits, deg	2.8−26	2.9−27.8
collected reflns	38 521	46 001
unique reflns (R_{int})	12 324 (0.073)	15 487 (0.058)
observed reflns $I > 2\sigma(I)$	4448	10 116
refined params	525	653
R(F)[a], $I > 2\sigma(I)$	0.0495	0.0439
wR(F^2)[a] (all data)	0.1156	0.1029

[a] $R(F) = \sum||F_o| - |F_c||/\sum|F_o|$, $wR(F^2) = [\sum w(F_o^2 - F_c^2)^2/\sum[w(F_o^2)]^{1/2}]$.

the Keggin subunits because bridging behavior is not observed, in contrast to the analogue dinuclear oxalate−copper complexes,[18] which afford extended monodimensional materials. Compounds **1** and **2** are the first discrete mono- and bimolecular TM-substituted Keggin POMs that support a binuclear copper−acetate complex.

Description of the Crystal Structures. The crystal structures of compounds **1** and **2** were determined by single-crystal X-ray diffraction (Table 1). Compound **1** contains the discrete hybrid polyanion $[\{SiW_{11}O_{39}Cu(H_2O)\}\{Cu_2(ac)_2(phen)_2(H_2O)\}]^{4-}$, which is made of a copper-monosubstituted α-Keggin polyanion as the inorganic building block and the Cu−phen−ac dimeric complex as the metalorganic one. This dimeric complex is anchored to the POM through an apical position, which is occupied by a POM terminal oxygen atom (Figure 1). The copper atom in the Keggin unit is disordered over the whole polyanion with the exception of the W1 and W2 positions. Thus, the dicopper complex and the POM are bound by a Cu−O−W bridge (138°), where the Cu1−O1 and W1−O1 bond lengths are 2.34 and 1.71 Å, respectively. On the other hand, compound **2** contains the dimeric hybrid polyanion $[\{Si_2W_{22}Cu_2O_{78}(H_2O)\}\{Cu_2(ac)_2(phen)_2(H_2O)\}_2]^{8-}$, which can be described as the condensation product of a couple of twofold-related $[\{SiW_{11}O_{39}Cu(H_2O)\}\{Cu_2(ac)_2(phen)_2(H_2O)\}]^{4-}$ units whose geometries are very similar to the above described geometry for compound **1** (Figure 2). Each α-Keggin subunit shows a preference site for the copper atom at the W12 octahedron with a population factor equal to 50%, which means the bridge between the subunits is always of type Cu−O−W (Cu12−O12−W12 = 166°). Although this type of TM−O−W bridge has been observed in cyclic[19] and chainlike polymolecular Keggin POMs with a TM = Mn^{II},[20] Co^{II},[21] or Cu^{II},[8a,22] to our knowledge there is only one other example of a bimolecular TM-disubstituted Keggin POM,[8b] which, unlike compound **2**, is not decorated with TM complexes. Table 2 displays ranges and mean values of M−O bond distances for both compounds and a comparison with the DFT-optimized copper-monosubstituted Keggin POM (DFT = density-functional theory).[8b]

The metalorganic building block is the same in both compounds and somewhat similar to the cationic species reported previously.[8b,23] It comprises two square-pyramidal Cu atoms bridged by two acetate ligands in a syn−syn fashion with a Cu−Cu distance close to 3.0 Å. Each basal plane is formed by two phenanthroline N atoms and two acetate O atoms, with the apical positions being occupied by the terminal oxygen atom of the W1 octahedron for Cu1 and a water molecule for Cu2. The phenanthroline ligands are almost parallel and are ring-to-bond stacked, with a torsion angle around 15° with respect to the Cu−Cu axis. This arrangement reveals intramolecular π interactions with average interplanar and intercentroidal distances of 3.35 and 3.70 Å, respectively. The ab initio optimized geometry[8b] of the $[\{Cu(phen)(H_2O)\}_2(ac)_2]^{2+}$ complex shows a twisted and open structure lacking an intramolecular $\pi-\pi$ interaction, whereas in all crystal structures containing this dicopper complex, the phenanthroline ligands are almost parallel disposed, favoring both intra- and intermolecular $\pi-\pi$ interactions. Selected bond lengths and angles for the metalorganic moieties are displayed in Table 3.

Despite the different nature of the POMs, the crystal packing of the two compounds is closely related, being formed of hybrid layers parallel to the *bc* plane that give rise to an alternate sequence of inorganic and metalorganic

(18) Reinoso, S.; Vitoria, P.; Lezama, L.; Luque, A.; Gutiérrez-Zorrilla, J. M. *Inorg. Chem.* **2003**, *42*, 3709.

(19) Kortz, U.; Matta, S. *Inorg. Chem.* **2001**, *40*, 815.

(20) Galán-Mascarós, J. R.; Giménez-Saiz, C.; Triki, S.; Gómez-García, C. J.; Coronado, E.; Ouahab, L. *Angew. Chem., Int. Ed. Engl.* **1995**, *34*, 1460.

(21) (a) Evans, H. T., Jr.; Weakley, T. J. R.; Jameson, G. B. *J. Chem. Soc., Dalton Trans.* **1996**, 2537. (b) Yan, B.; Xu, Y.; Bu, X.; Goh, N. K.; Chia, L. S.; Stucky, G. D. *J. Chem. Soc., Dalton Trans.* **2001**, 2009.

(22) Lisnard, L.; Dolbecq, A.; Mialane, P.; Marrot, J.; Sécheresse, F. *Inorg. Chim. Acta* **2004**, *357*, 845.

(23) Tokii, T.; Watanabe, N.; Nakashima, M.; Muto, Y.; Morooka, M.; Ohba, S.; Saito, Y. *Bull. Chem. Soc. Jpn.* **1990**, *63*, 364.

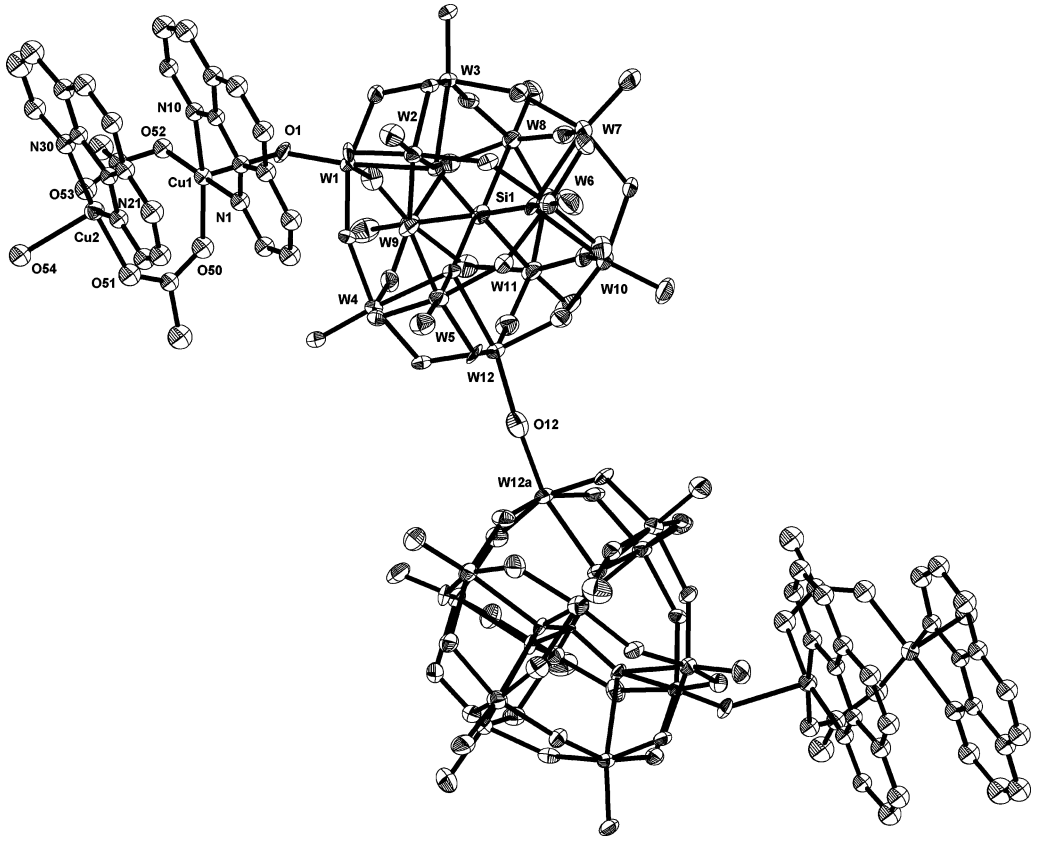

Figure 2. ORTEP view of metalorganic−POM hybrid of compound **2** with atom labeling.

Table 2. Ranges and (Mean) M−O Bond Distances [Å] for the POM of Compounds **1**, **2**, and the DFT-Optimized Copper-Monosubstituted Keggin Polyanion

	1	**2**[a]		optimized polyanion	
	$[SiW_{11}O_{39}Cu(H_2O)]^{6-}$	$[Si_2W_{22}Cu_2O_{78}(H_2O)]^{12-}$		$[SiW_{11}O_{39}Cu(H_2O)]^{6-}$	
		W^{VI}	Cu^{II}	W^{VI}	Cu^{II}
$M-O_a$[b]	2.29−2.36 (2.34)	2.305−2.384 (2.338)	2.366	2.32−2.44 (2.39)	2.319
$M-O_b$[b]	1.84−2.00 (1.91)	1.858−1.965 (1.908)	1.927, 1.932	1.81−2.03 (1.93)	2.011
$M-O_c$[b]	1.87−1.97 (1.92)	1.842−1.998 (1.928)	1.965, 1.980	1.82−2.03 (1.94)	2.018
$M-O_t$[b]	1.66−1.78 (1.72)	1.706−1.755 (1.725)	1.972	1.76−1.77 (1.77)	2.286
$Si-O_a$[b]	1.61−1.67 (1.64)	1.612−1.641 (1.628)		1.63−1.66 (1.65)	
M···Si	3.48−3.55 (3.52)	3.510−3.555 (3.525)	3.493	3.56−3.64 (3.60)	3.377
$M\cdots M_{trans}$	7.00−7.07 (7.04)	7.027−7.069 (7.046)	7.013	7.15−7.21 (7.19)	6.964
$O\cdots O_{trans}$	10.31−10.49 (10.41)	10.407−10.450 (10.429)	10.669	10.61−10.69 (10.66)	10.709

[a] Cu^{II} site corresponds to the W12 octahedron with a population factor of 50%. [b] O_a, oxygen atoms belonging to the central SiO_4 tetrahedron; O_b, bridging oxygen atoms between corner-sharing MO_6 octahedra; O_c, bridging oxygen atoms between edge-sharing MO_6 octahedra; O_t, terminal oxygen atoms.

regions along the *a* axis, as can be seen from the relationship between the crystal parameters of both structures (Figure 3). The inorganic region of compound **1** can be described as zigzag chains of 2_1-axis related hybrid polyanions along the *b* axis, which are cemented by potassium cations and water molecules through an extended hydrogen bonding network that involves the potassium-coordinated water molecules and the POM terminal oxygen atoms. On the other hand, in compound **2** the bimolecular hybrid polyanions are disposed parallel to each other and are probably interconnected by an extended network of potassium cations and water molecules, leading also to a row along the *b* axis. In both compounds, the metalorganic moieties are disposed pointing up and down the *ab* plane.

In both compounds, the dicopper complexes establish a very similar and extensive network of intermolecular interactions (Figure 4). The C−H···O interactions between phenanthroline aromatic rings and POM surface oxygen are depicted in the d_e Hirshfeld surface as red hollows (bottom left), and the inter- and intramolecular π interactions between the phenanthroline ligands are nicely represented by the characteristic blue and red alternating triangles on the shape-index Hirshfeld surfaces (bottom center and right).

This very remarkable similarity is also observed in the Hirshfeld surfaces of the supported cation moieties (Figure 5). Thus, in the metalorganic regions, each copper complex is involved on one hand in intermolecular $\pi-\pi$ and $C-H\cdots O_w$ interactions with the centrosymmetrically related copper complex, as displayed in Figure 5a by the large flat surface on the curvedness plot combined with the characteristic alternating rhombus-shaped red and blue regions of the shape index. Moreover, it also interacts through weaker

Table 3. Bond Distances [Å] and Angles [deg] for the Experimental and DFT-Optimized $[Cu_2(ac)_2(phen)_2(H_2O)]^{2+}$ Building Blocks in Compounds **1** and **2**

Cu1 coordination sphere			Cu2 coordination sphere			
compound	**1**	**2**		**1**	**2**	optimized[a]
			Bond Lengths			
Cu1−O50	1.97(1)	1.978(8)	Cu2−O51	1.93(2)	1.938(9)	1.931
Cu1−O52	1.90(1)	1.947(8)	Cu2−O53	1.94(1)	1.976(8)	1.951
Cu1−N1	1.98(2)	1.998(9)	Cu2−N21	2.00(2)	1.997(9)	2.008
Cu1−N10	1.99(2)	1.997(9)	Cu2−N30	2.00(2)	1.987(9)	2.006
Cu1−O1	2.34(1)	2.291(8)	Cu2−O54	2.20(1)	2.213(8)	2.290
Cu1···Cu2	2.994(4)			2.997(2)		3.300
			Bond Angles			
O50−Cu1−O52	91.4(6)	91.6(3)	O51−Cu2−O53	90.2(6)	91.7(3)	92.7
O50−Cu1−N10	167.4(6)	167.9(3)	O51−Cu2−N30	173.9(6)	172.3(4)	167.2
O50−Cu1−O1	97.4(5)	95.4(3)	O51−Cu2−O54	90.8(6)	87.7(3)	97.5
O52−Cu1−N1	173.9(7)	174.4(4)	O53−Cu2−N21	165.9(6)	164.5(3)	173.1
O52−Cu1−O1	94.1(5)	94.0(3)	O53−Cu2−O54	92.4(5)	91.5(3)	81.6
N1−Cu1−N10	80.4(7)	81.8(4)	N21−Cu2−N30	83.2(7)	81.9(4)	83.0
			Dihedral Angles[b]			
Cu1−phen1	6.0(5)	6.7(3)	Cu2−phen2	15.0(5)	13.1(3)	6.7
Cu1−Cu2	22.4(6)	21.4(3)				41.6
phen1−phen2	3.2(4)	3.3(2)				44.4
			Torsion Angles[c]			
phen1−phen2	15.4(6)	15.2(3)				25.2

[a] Optimized as the $[\{Cu(phen)(H_2O)\}_2(ac)_2]^{2+}$ cation. [b] Basal planes. Cu1: O50, O52, N1, N10. Cu2: O51, O53, N21, N30. Aromatic ring planes. phen1: N1, N10, C2−C14. phen2: N21, N30, C22−C34. [c] Torsion angle defined as the mean value of the following angles: C13−Cu1−Cu2−C33 and C14−Cu1−Cu2−C34.

Table 4. Intra- and Intermolecular π Interactions Involving the Metalorganic Complexes in Compounds **1** and **2**

π-interaction type[a]			DZ	ANG	DC	DXY
intramolecular	**1**	Cg1−Cg2	3.36(1)	3.4(6)	3.71(1)	1.53(1)
	2	Cg1−Cg2	3.34(1)	3.1(4)	3.71(1)	1.62(1)
intermolecular dimer−dimer	**1**	CgN21−CgN21′[b]	3.43(1)	0.0(7)	3.69(1)	1.36(1)
		CgN21−CgC2′[b]	3.44(1)	1.6(7)	3.56(1)	0.91(1)
		CgC2−CgN21′[b]	3.41(1)	1.6(8)	3.56(1)	1.02(2)
	2	CgN21−CgN21′[c]	3.413(7)	0.0(4)	3.599(7)	1.142(7)
		CgN21−CgC2′[c]	3.407(6)	3.3(4)	3.576(6)	1.086(6)
		CgC2−CgN21′[c]	3.347(6)	3.3(4)	3.576(6)	1.259(6)
intermolecular dimer−Keggin	**1**	CgN1−TET	2.82(1)	14.8(7)		
	2	CgN1−TET	2.823(7)	15.0(4)		

[a] Cg*i*: centroid of ring defined by the following atoms. *i* = N21: N21, C22, C23, C24, C31, C33. *i* = C2: C33, C34, C32, C26, C25, C31. *i* = N1: N1, C2, C3, C4, C11, C13. TET: mean plane of the tetramer W(1,2,3,4) defined by the oxygen atoms O1, O16, O4, O22, O5, O17, O2, and O13. DZ: perpendicular distance of Cg*i* on plane *j*. ANG: dihedral angle between planes *i* and *j*. DC: distance between ring centroids. DXY: distance (Å) between Cg*j* and the projection of Cg*i* onto the plane *j*. [b,c] Symmetry codes: (b) $-x, 2-y, -z$; (c) $1/2-x, 1/2-y, 1-z$.

C−H···π and C−H···H−C interactions with four other neighbor complexes. On the other hand, the twisted conformation of the dicopper complex allows one of its phenanthroline ligands to interact with the terminal and bridging oxygen atoms belonging to a W_4O_{18} tetramer of the POM on which it is supported, as shown in Figure 5b by the multiple red and blue hollows in the d_e and shape-index plots, respectively. This type of interaction avoids the formation of infinite columns of π-stacked complexes, which are present in the packing of the related ionic derivatives. Moreover, the complexes form weaker C−H···O interactions with three other neighboring POMs. A further connection between the inorganic and metalorganic regions is established by means of a hydrogen bond between the apical water molecule of the metalorganic moiety and a terminal oxygen belonging to an adjacent POM [O3···O54, 2.82 (**1**) and 2.75 Å (**2**); Figure 5a].

Table 4 summarizes the intra- and intermolecular contacts involving the supported dinuclear complexes.

EPR Spectroscopy. X-band powder EPR spectra of compound **2** recorded at different temperatures between 4.2 and 290 K are illustrated in Figure 6. Similar results (included as Supporting Information) were obtained for compound **1**, in good agreement with the close geometry of the hybrid polyanions in both compounds. The room-temperature X-band spectrum displays a broad anisotropic resonance centered at about 3200 G, together with a set of three less intense signals observed at about 1500, 2400, and 4000 G. This set of signals can be associated with a well-isolated triplet spin state showing a relatively small zero-field splitting, and, therefore, it must be originated by the Cu^{II} dimer. The low-field signal corresponds to a $\Delta M_S = \pm 2$ forbidden transition. Their intensity diminishes as the temperature is lowered, and they vanish below 10 K, in line with the strong antiferromagnetic coupling expected in the dimer.

On the other hand, lowering the temperature of the samples results in better resolution of the central (3200 G) resonance.

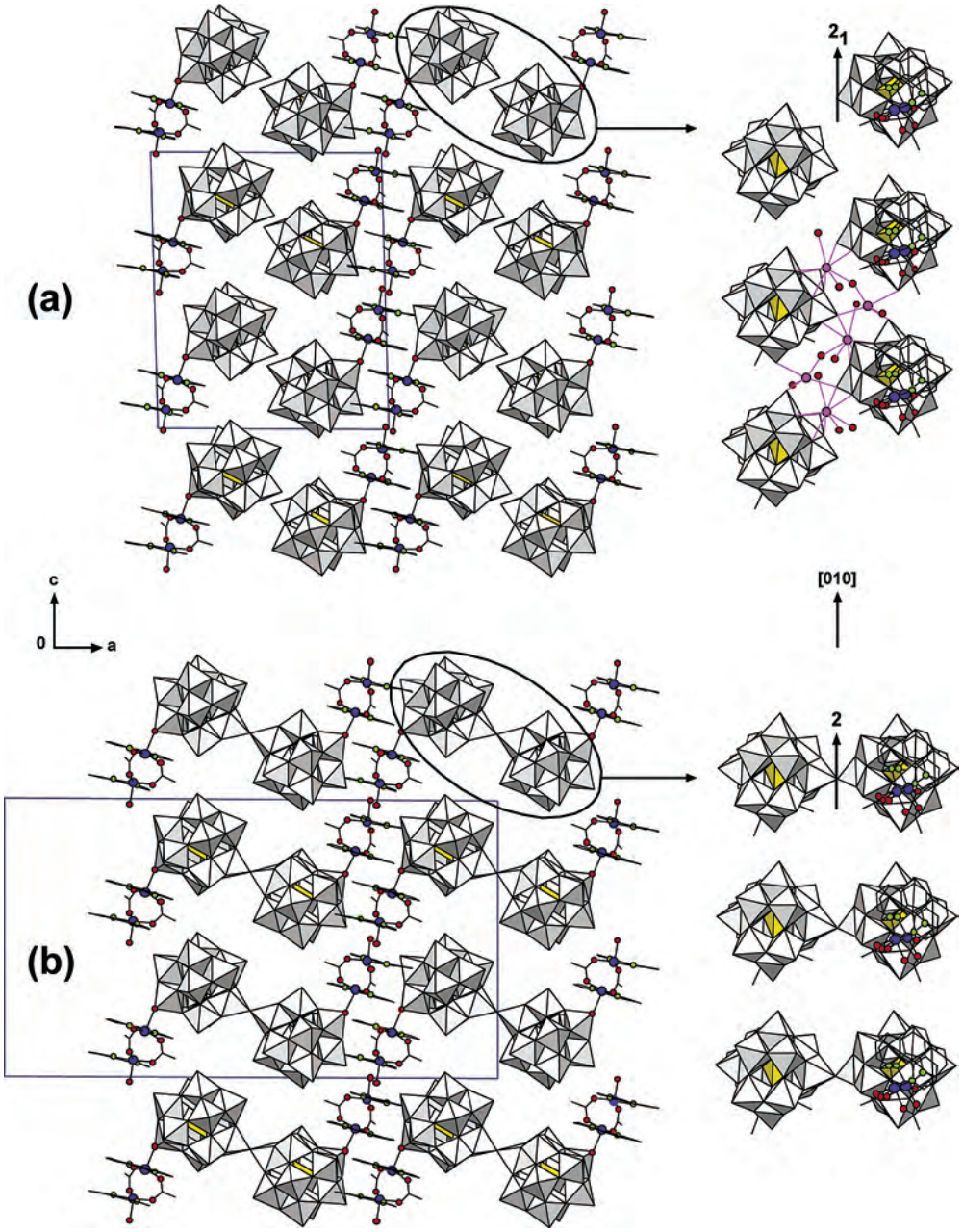

Figure 3. Views along the crystallographic *b* axis showing the presence of metalorganic layers formed by π-stacked POM-supported $[Cu_2(ac)_2(phen)_2(H_2O)]^{2+}$ moieties, alternating with inorganic layers of the cluster anions $[SiW_{11}O_{39}Cu(H_2O)]^{6-}$ in compound **1** (top) or $[Si_2W_{22}Cu_2O_{78}(H_2O)]^{12-}$ in compound **2** (bottom). Alkaline cations and lattice water molecules are not shown for clarity.

Below 50 K, it gives rise to a signal with a partially resolved hyperfine structure on the parallel region. This signal can be ascribed to an isolated Cu^{II} chromophore with an axial **g** tensor and, therefore, it must be originated by the Cu^{II}-monosubstituted Keggin subunits. The spin Hamiltonian parameters of this monomeric contribution were estimated by the comparison of the low-temperature X-band spectrum with that generated by a computer simulation program working at the second order of the perturbation theory. The values obtained for the principal components of the **g** and **A** tensors (Table 5) are in good agreement with those observed in previously analyzed analogous systems.[18,24] They are typical of octahedrally coordinated Cu^{II} ions with the unpaired electron on the $d_{x^2-y^2}$ orbital. Moreover, the high $g_{\parallel}$ value indicates a low Jahn−Teller distortion associated to the Cu^{II} ion due to the rigidity imposed on its coordination sphere by the pentadentate monolacunary Keggin ligand.

The severe overlap of the individual lines in the $\Delta M_S = \pm 1$ region precludes any attempt to extract the principal components of the **g** tensor of the dimeric contribution or to evaluate its zero-field splitting from the X-band spectra. Q-band EPR experiments were, therefore, performed between 120 and 290 K, which led to a considerable improvement of the resolution of the spectra (Figure 7). In addition to the half-field signal (ca. 5700 G), at least six more lines can be detected between 9000 and 13 000 G, which show no

(24) (a) Scholz, G.; Lück, R.; Stösser, R.; Lunk, H.-J.; Ritschl, F. *J. Chem. Soc., Faraday Trans.* **1991**, *87*, 717. (b) Gamelas, J. A.; Santos, I. C. M. S.; Freire, C.; de Castro, B.; Cavaleiro, A. M. V. *Polyhedron* **1999**, *18*, 1163.

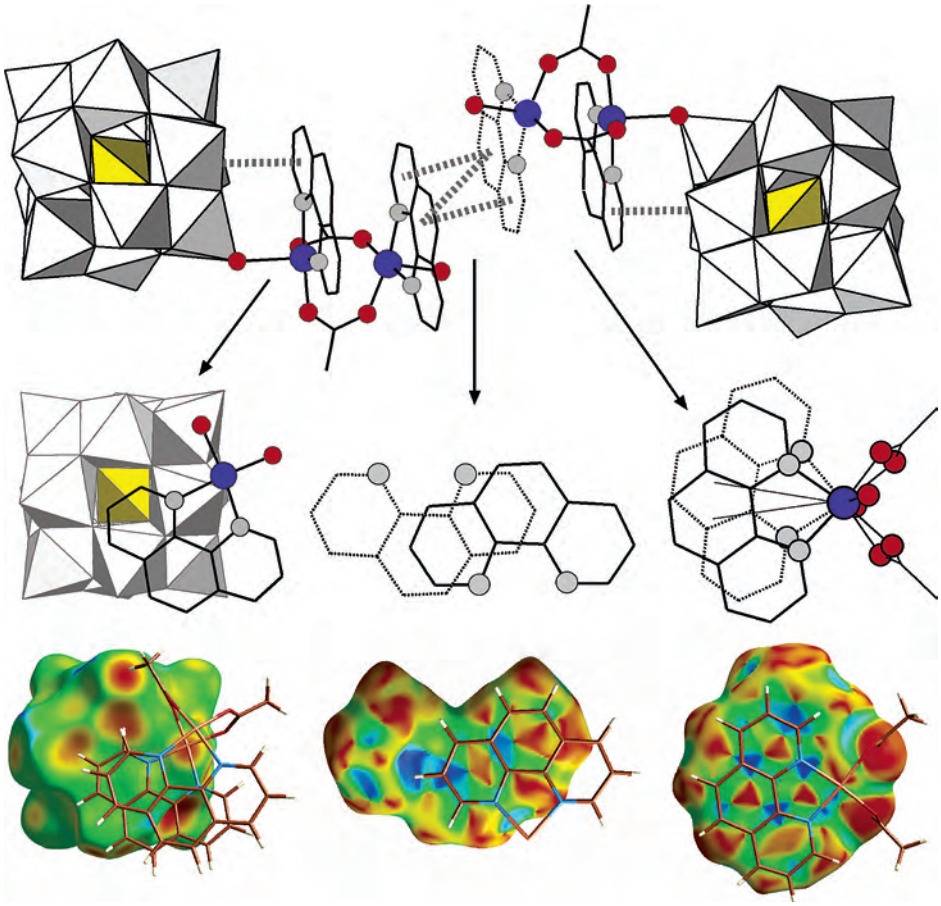

Figure 4. Representation of the different types of π interactions present in compounds **1** and **2**. From left to right are $\pi-$tetramer, intermolecular $\pi-\pi$, and intramolecular $\pi-\pi$ interactions. Top: combined polyhedral and ball-and-stick views. Bottom: Hirshfeld surfaces mapped with d_e [left, mapped between 1.1 (red) and 3.1 Å (blue)] and shape index (center and right).

Table 5. Spin Hamiltonian Parameters for Copper(II) Centers Present in Compounds **1** and **2**

	compound **1**			compound **2**		
	Q (120 K)	X (290 K)	X (4.2 K)	Q (120 K)	X (290 K)	X (4.2 K)
			$\{Cu_2(phen)_2(ac)_2\}^{2+}$			
$g_{\parallel}$	2.260	2.260		2.260	2.260	
$g_{\perp}$	2.065	2.060		2.064	2.057	
$\langle g \rangle$	2.130	2.127		2.129	2.125	
D (cm^{-1})	0.130	0.135		0.131	0.135	
			$\{SiW_{11}O_{39}Cu(H_2O)\}^{6-}$			
$g_{\parallel}$	2.425	2.425	2.425	2.412	2.428	2.428
$g_{\perp}$	2.095	2.105	2.105	2.092	2.095	2.095
$\langle g \rangle$	2.205	2.212	2.212	2.199	2.206	2.206
$A_{\parallel}$ ($\times 10^{-4}$ cm^{-1})	100	100	100	100	100	100
$A_{\perp}$ ($\times 10^{-4}$ cm^{-1})	28	28	28	28	28	28

substantial modifications as the temperature is lowered. Two of them are associated with the monomeric contribution, and they were simulated as an axial signal by using the spin Hamiltonian parameters given in Table 5. The rest of the observed resonances correspond to the dimeric contribution, and they were simulated as a triplet spin state with collinear **D** and **g** tensors of axial symmetry ($E = 0$). A reasonable fit was achieved by using the reported formulas for the transition fields along the principal axes.[25] The values obtained for the principal components of the **g** tensor are consistent with the structural characteristics of the dimer. They are typical of a Cu^{II} ion in a square-pyramidal environment, with the unpaired electron on the $d_{x^2-y^2}$ orbital. Moreover, the small zero-field splitting is in good agreement with that observed in related Cu^{II} dimers with two bridging carboxylate ligands in a syn−syn fashion.[26] The fit of all signals was satisfactory with the exception of a central line (ca. 11 300 G), which can be assigned to a forbidden double-quantum transition, although it could also be originated by the small noncoupled paramagnetic impurity observed in the magnetic susceptibility measurements. The room-temperature X-band spectrum

(25) Wasserman, E.; Snyder, L. C.; Yager, W. A. *J. Chem. Phys.* **1964**, *41*, 1763.

(26) (a) Battaglia, L. P.; Corradi, A. B.; Ianelli, S.; Zoroddu, M. A.; Sanna, G. *J. Chem. Soc., Faraday Trans.* **1991**, *87*, 3863. (b) Costa, R.; López, C.; Molins, E.; Espinosa, E. *Inorg. Chem.* **1998**, *37*, 5686.

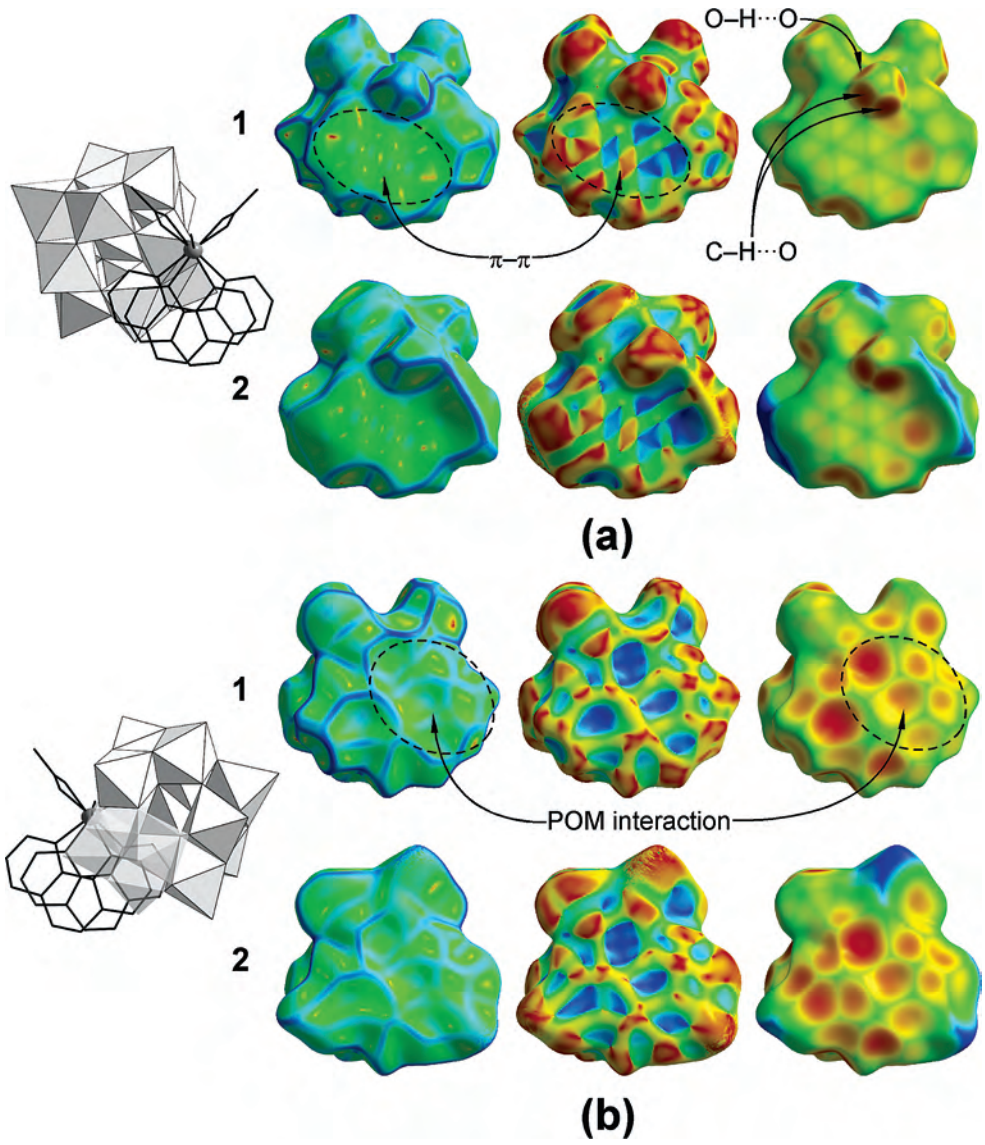

Figure 5. Hirshfeld surfaces of $[Cu_2(ac)_2(phen)_2(H_2O)]^{2+}$ moieties for compounds **1** and **2**. Each cation is shown with the surface mapped with curvedness (left), shape index (center), and d_e [right, mapped between 1.1 (red) and 3.1 Å (blue)]. (a) Detail of the interactions (mainly $\pi-\pi$) with the centrosymmetric-related cation. (b) View showing the interactions with the supporting POM. The slightly different global shape and bigger volume of the Hirshfeld surface for compound **2** are due to the applied Platon/Squeeze procedure.

was also fitted following the same procedure, and the obtained results are similar to those extracted from the Q-band spectra (Table 5).

The thermal evolution of the magnetic molar susceptibility and the $\chi_m T$ product ($\chi_m T = \mu_{eff}^2/8$) for compounds **1** and **2** is displayed in Figure 8. The magnetic behaviors of both compounds show similar trends: the χ_m curve increases continuously with decreasing temperature, and no maximum is observed. At high temperature ($T > 200$ K), the susceptibility data are well-described by means of Curie−Weiss expressions, being $C_m = 1.34$ cm^3·K·mol^{-1} and $\theta = -36.3$ K for **1** and $C_m = 2.69$ cm^3·K·mol^{-1} and $\theta = -35.6$ K for **2**.

The values of $\chi_m T$ at 300 K are 1.200 cm^3·K·mol^{-1} for compound **1** and 2.406 cm^3·K·mol^{-1} for compound **2**, which are in good agreement with the presence of three and six noncorrelated Cu^{II} ions per formula unit, respectively (1.125 and 2.250 cm^3·K·mol^{-1}, considering $g = 2$). When the systems are cooled, the $\chi_m T$ product decreases from 300 to about 20 K, remaining approximately constant below 20 K. The values of $\chi_m T$ at 5 K are 0.473 cm^3·K·mol^{-1} for compound **1** and 0.936 cm^3·K·mol^{-1} for compound **2**, which correspond to one and two noncorrelated Cu^{II} ions, respectively. This behavior indicates the presence of relatively strong antiferromagnetic interactions between the Cu^{II} ions forming part of the dimeric complexes, whereas the Cu^{II}-monosubstituted Keggin subunits show a paramagnetic contribution, which predominates below 20 K and masks any possible maximum of the χ_m curve.

The experimental curves have been compared with those calculated with the following general expression:

$$\chi_m = A\left[\frac{(1-\rho)Ng^2\beta^2}{kT[3+\exp(-J/kT)]} + \frac{\rho Ng^2\beta^2}{4kT}\right] + B\frac{Ng'^2\beta^2}{4kT} \quad (1)$$

where N, β, and k have their usual meaning, g is the average g factor of the copper−acetate−phenanthroline complexes,

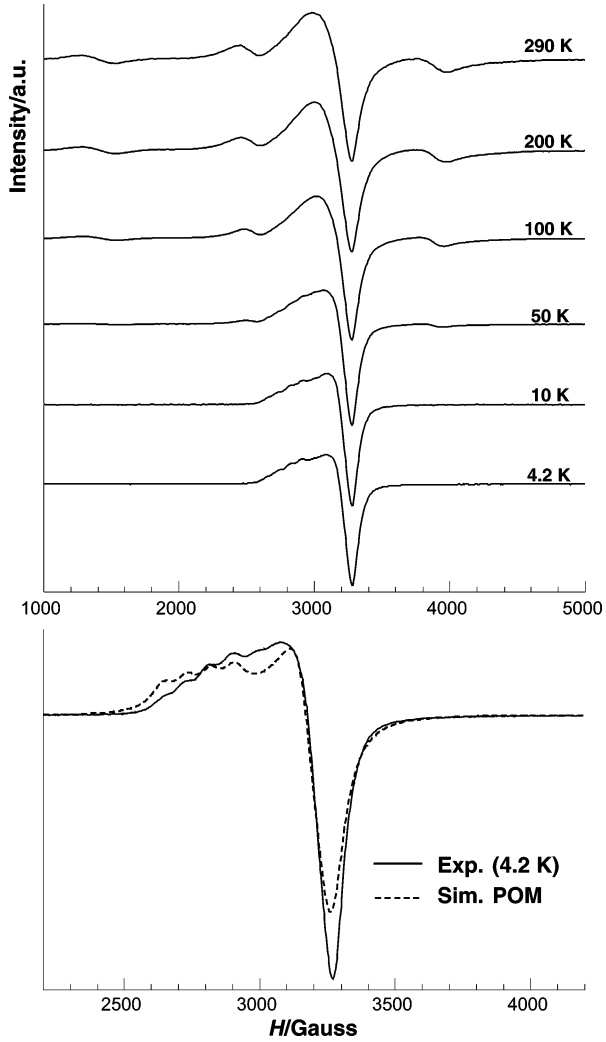

Figure 6. Top: Temperature dependence from 4.2 to 290 K of the X-band EPR powder spectra of compound **2**. Bottom: Detail of the low-temperature X-band EPR powder spectrum of compound **2**. The dashed line corresponds to the simulated spectrum for an isolated Cu^{II} ion.

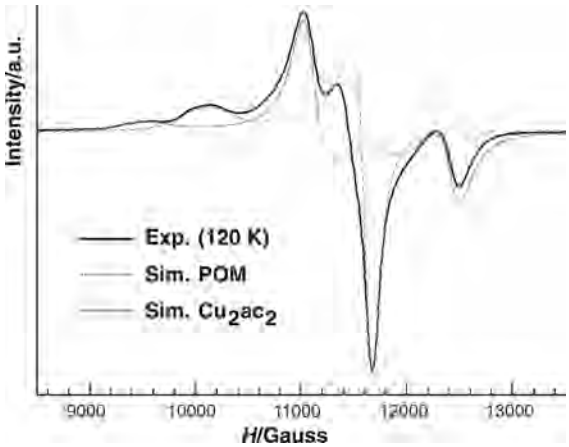

Figure 7. Q-band EPR powder spectrum of compound **2** at 120 K. Thin lines correspond to the simulated spectra for an isolated Cu^{II} ion (dashed line) and for an isolated triplet spin state with collinear **D** and **g** tensors of axial symmetry (continuous line).

and g' is the local g factor of the Cu^{II}-monosubstituted Keggin POMs.

The first term in the above equation is the classical Bleaney−Bowers equation for a dinuclear Cu^{II} complex[27]

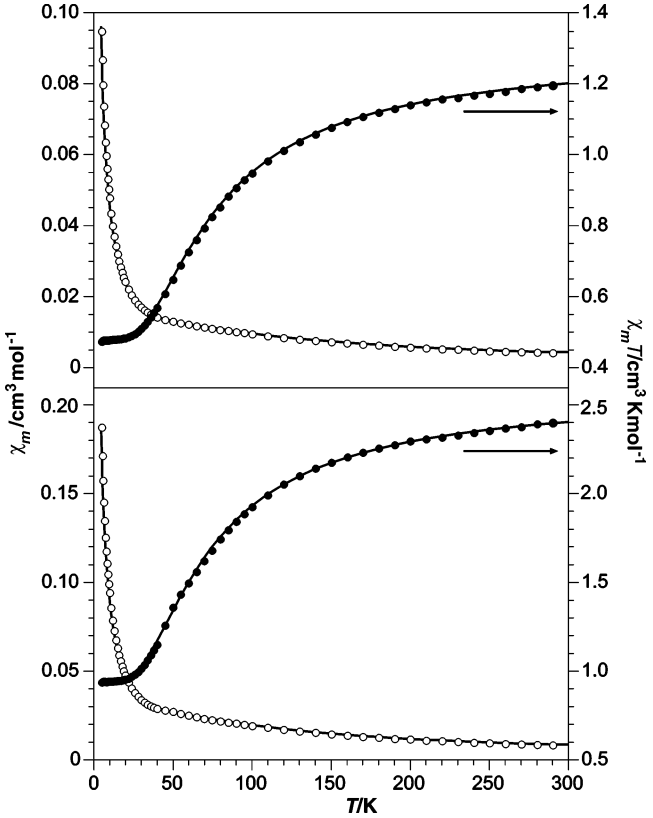

Figure 8. Thermal evolution of the magnetic susceptibility and $\chi_m T$ product for compounds **1** (top) and **2** (bottom). Continuous lines represent the least-squares fit to eq 1.

expressed per copper atom and modified to take into account the presence of noncoupled impurities. The singlet−triplet energy gap (J) is defined by the Hamiltonian $H = -JS_AS_B$ ($S_A = S_B = 1/2$), and ρ is the percent of noncoupled impurity. The last term corresponds to the paramagnetic contribution of the Cu^{II}-monosubstituted POMs. The A and B factors represent the number of Cu^{II} ions belonging to the dimeric and monomeric species, respectively (**1**, $A = 2$ and $B = 1$; **2**, $A = 4$ and $B = 2$).

Least-squares fits of eq 1 to the data were performed by minimizing the following function:

$$R = \left\{ \sum_{i=1}^{NP} [\chi_m(\mathrm{exp})_i - \chi_m(\mathrm{cal})_i]^2/(\mathrm{NP} - \mathrm{NV}) \right\}^{1/2} \qquad (2)$$

where NP is the number of data points and NV is the number of variable parameters. The best fit results are $J = -97.5$ cm^{-1}, $g = 2.13$, $g' = 2.20$, $\rho = 2.7\%$, and $R = 3.12 \times 10^{-4}$ for compound **1** and $J = -92.1$ cm^{-1}, $g = 2.13$, $g' = 2.19$, $\rho = 2.4\%$, and $R = 3.09 \times 10^{-4}$ for compound **2**. The calculated J values are very similar for compounds **1** and **2**, as it was expected from the almost identical structural parameters the Cu^{II} dimers show in both compounds. They are in concordance with the deduced Weiss temperatures, which must be approximately one-fourth of the exchange integrals for dimeric systems with $S = 1/2$.[28] Moreover, the obtained g factors closely reproduce the mean g values

(27) Bleaney, B.; Bowers, K. D. *Proc. R. Soc. London, Ser. A* **1952**, *214*, 451.

deduced from the EPR spectroscopy for both dimeric and monomeric species.

On the other hand, the obtained coupling constants are in good agreement with both the observed and the DFT-calculated singlet−triplet energy gap for the $[Cu_2(ac)_2(phen)_2(H_2O)_2]^{2+}$ complex cation in the nitrate[23,29] or in the $[Si_2W_{22}Cu_2O_{78}(H_2O)]^{12-}$ POM[8b] salts. This fact indicates that the apical coordination of the Cu^{II} dimer to the Cu^{II}-monosubstituted Keggin subunits that takes place in compounds **1** and **2** has almost no influence in the magnitude of the antiferromagnetic coupling.

Conclusions

The reactions between in situ generated copper-monosubstituted Keggin POM and copper−phenanthroline complexes in acetic acid/alkaline acetate buffers afford different hybrid inorganic−metalorganic compounds, depending on the nature of the alkaline cation. When Rb^+ or NH_4^+ acetate buffers are used, the $[\{Cu(phen)(H_2O)\}_2(ac)_2]^{2+}$ dimer remains as the countercation to give ionic compounds, whereas in the research described in this article, when Na^+ or K^+ acetate media are used, the dimer gets anchored to the Keggin subunits to give discrete hybrid polyanions. Compounds **1** and **2** are the first mono- and bimolecular TM-substituted Keggin POMs that support a binuclear copper−acetate complex.

Both compounds display a layered crystal structure in which an alternate sequence of inorganic and metalorganic regions can be observed. The dicopper complexes, which are very similarly supported on the Keggin units and show a very close geometry, establish an extensive network of intermolecular interactions, which gives almost identical metalorganic regions in both crystal structures. From this fact, it can be inferred that the inorganic components of the structure, despite their different nature, are forced to accommodate in such a way that this network of directional and structure-directing[30] intermolecular interactions established by the copper complexes is maximized.

EPR studies show a strong antiferromagnetic coupling between the copper atoms in the $[Cu_2(ac)_2(phen)_2(H_2O)]^{2+}$-supported complexes and the presence of magnetically isolated copper atoms in each Keggin subunit of the POMs. This fact is confirmed by magnetic susceptibility studies, which also show that the coordination of the dinuclear complex to the POM has negligible influence in the magnitude of the antiferromagnetic coupling.

Acknowledgment. The authors thank Universidad del País Vasco (9/UPV00169.310-15329/2003) and Ministerio de Ciencia y Tecnología (MAT2005-03047) for financial support and Prof. D. Jayatilaka for the Crystal Explorer program. S.R. thanks Gobierno Vasco for his Doctoral Fellowship.

Supporting Information Available: Detailed views of the dicopper complexes and the hybrid layers with selected geometrical parameters, Hirshfeld surface fingerprint plots of the dicopper complexes, X- and Q-band EPR experimental and simulated spectra of compound **1**, and X-ray crystallographic files of compounds **1** and **2** in CIF format. This material is available free of charge via the Internet at http://pubs.acs.org.

IC051322C

(28) Carlin, R. L. *Magnetochemistry*; Spinger-Verlag: Berlin, 1986.
(29) Rodríguez-Fortea, A.; Alemany, P.; Alvarez, E.; Ruiz, S. *Chem.—Eur. J.* **2001**, *7*, 627.
(30) (a) Hunter, C. A.; Sanders, J. K. M. *J. Am. Chem. Soc.* **1990**, *112*, 5525. (b) Janiak, C. *J. Chem. Soc., Dalton Trans.* **2000**, 3885. (c) Hunter, C. A.; Lawson, K. R.; Perkins, J.; Urch, C. J. *J. Chem. Soc., Perkin Trans. 2* **2001**, 651.